

Wavepath tomography for model building and hazard detection

D. Bevc (3DGeo Inc.), M.M. Fliedner (3DGeo Inc.) & B. Biondi (Stanford University)*

Summary

In complex velocity models, such as below rugose salt bodies, wavefield continuation migration is usually superior to Kirchhoff methods because of multi-pathing, sharp velocity contrasts and the bandlimited nature of seismic wave propagation. Wavepath tomography offers a way to build the velocity model in a way that is consistent with the migration operator: instead of tracing rays to backproject residual velocities, a "wavepath" is constructed using the actual wavefield continuation operator to represent the wave propagation between surface source/receiver pairs and subsurface reflection points by multiplication of impulse responses downgoing from the surface location and upgoing from the reflection point. The size of the inversion is kept manageable by restricting the wavepath to the first Fresnel zone. We demonstrate the applicability and superiority of this approach for building complex velocity models in areas of salt tectonics and for hazard detection.

Introduction

In regions of structural complexity such as below rugose salt bodies, raytracing based tomographic velocity model updating suffers from similar problems as Kirchhoff migration: it may not be possible to trace rays through certain parts of the model and multipathing is not easy to take into account. Wavefield continuation imaging methods, such as common azimuth or shot profile migration overcome these shortcomings naturally. It is therefore desirable to base the velocity model building on the same methods. Wavepath tomography replaces backprojection of velocity errors along rays with backprojection along wavepaths that are generated with the same propagation operator as the seismic image. In this paper we describe the method of wavepath tomography with synthetic 2D examples. The process, however, is formulated and implemented in 3D.

Methodology: Automated Tomography

To streamline the velocity model updating process, we have implemented an automatic method of signal detection that eliminates the need for manual reflector picking by scanning the seismic data volume with prediction-error filters and automatically selecting back projection points based on dip coherency and semblance strength (Bevc et al. 2006; Clapp et al. 1998). This approach can save months of human time on a typical 3D seismic imaging project and, thereby, shortens seismic imaging project turnaround time while exploiting the full redundancy of the recorded data. The automation also reduces human bias and manual picking error, while retaining the option to control quality and steer the solution. This approach is used with both standard tomographic ray-trace updating, and the wavepath method described herein.

Selecting backprojection points independent of manually picked horizons involves calculating the best single dip in a window and the coherency of the dip by iterative application of plane-wave destruction filters. Points that satisfy specified levels of dip coherency, amplitude, semblance strength, and distance from other points and the edges of the image are selected as backprojection points. This method allows for an even distribution of backprojection points in the absence of strong geological boundaries (reflectors) that define the velocity model.

Methodology: Wavepath

Wavepath tomography is based on an idea by Woodward (1989): instead of tracing rays to backproject residual velocities, a "wavepath" is constructed using the actual wavefield continuation operator to represent the wave propagation between surface source/receiver pairs and subsurface reflection points. In this way multi-pathing, sharp velocity contrasts, and the bandlimited nature of seismic wave propagation can be modeled more naturally than with geometric rays.

To create a wavepath for a given velocity model, the impulse responses of the wavefield propagator are calculated for a source at the desired surface location (downgoing wavefield) and at the reflection point (upgoing wavefield) for one frequency. The two wavefields are then multiplied and the imaginary part of the product is retained. By adding kernels for several frequencies, the bandwidth of the seismic image can be faithfully represented, but for velocity model building, a single central frequency is usually sufficient.

In order to achieve a compact wavepath and thereby minimize the size of the inversion problem, the kernel outside a volume like the first Fresnel zone is zeroed. This can be achieved simply by thresholding the wavepath amplitude, tracking the central zero crossing, or employing a pseudo-eikonal event tracker (Brown et al. 2006) by treating the kernel as a pseudo-velocity field. The latter method works especially well in 3D.

Methodology: Backprojection

The proper inversion weights for the tomographic velocity update can be easily understood by considering the ray analogy: In the ray approximation, the inversion weights a_{ij} of the inversion matrix A in $A\Delta s = \Delta \tau$ represent the length of raypath segments for each slowness cell traversed by a ray, the row sum is therefore equal to the ray length l . For a wavepath of unit amplitude everywhere over its support, the row sum equals its volume V . Consequently, the average weight is $a_{ij}=l/V$. Without changing the row sum, each individual weight can be modified according to the actual amplitude of the wavepath kernel.

Example: Sigsbee subsalt velocity update

As an example, we show a tomographic update of the subsalt region in the Sigsbee velocity model. The starting migration velocity is correct down to base salt and constant below. A fairly small number of backprojection points is selected (Fig. 1 left) based on reflection and semblance strengths, and reflector coherency (Bevc et al. 2006). Examples of normal incidence wavepaths are shown on the right side of Fig. 1 (offset wavepaths, where source and receiver surface location are separate, are not shown for this example). In contrast to infinitely narrow raypaths, the width of the wavepaths provides a natural regularization of the inversion. The updated velocity model (Fig. 2 left) is smoothed to compensate for the considerable gaps in backprojection point coverage. The result is comparable with what can be achieved with ray tomography using the same residual data, but with 20 times the number of rays (normal and oblique incidence).

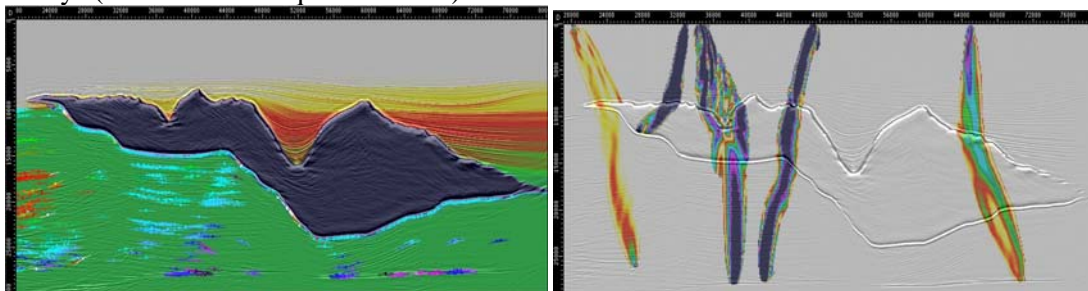


Figure 1: Sigsbee synthetic model; starting velocity model (constant below salt) and backprojection points (color indicates velocity residual) overlaid on seismic image (left); selected normal incidence wavepaths through the starting model (right).

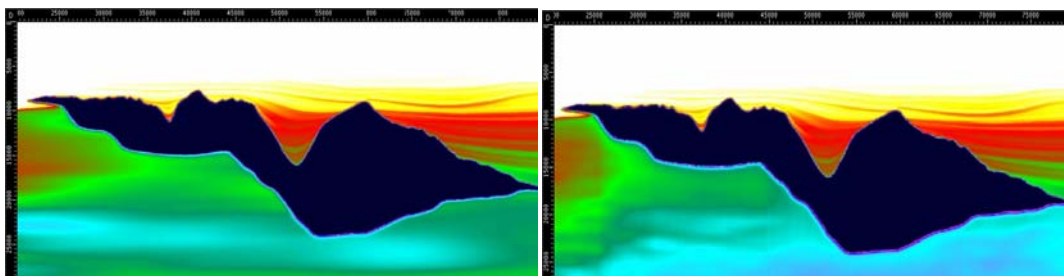


Figure 2: two iterations wavepath tomography of Sigsbee starting velocity model (Fig. 1).

A further iteration (Fig. 2 right) brings the subsalt velocity model into agreement with the actual background model so that the flat subsalt reflector is positioned correctly and major subsalt faults and point diffractors are better resolved (Fig. 3).

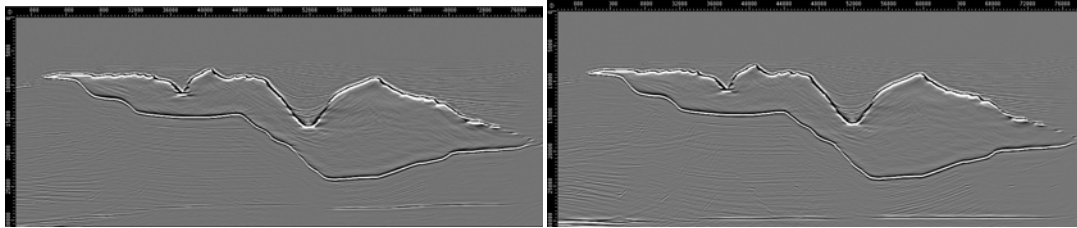


Figure 3: Sigsbee seismic image with starting velocity model (left) and after velocity updates (right).

Subsalt Hazard Detection

As a test case that combines the techniques described in the previous section, we choose a widely used 2D synthetic dataset provided by BP (Fig. 4). Our target is the narrow low-velocity anomaly below the left salt body. For the starting model we assume that the velocity above salt and the salt bodies are known exactly whereas the velocity below salt is a simple gradient extended laterally from the center of the section (Fig. 4). The ratio between starting and true velocity ranges from 0.76 to 1.57.

We migrate the synthetic data with a common-azimuth algorithm (Biondi and Palacharla 1996) using a phase-shift downward continuation operator. Reflector continuity in the zone of interest is very poor, which is also reflected in the low semblance strength of the common image gathers (CIGs) below salt. Starting from the dip fields of stack and CIGs, we generate automatic picks of backprojection points, reflector normal directions, and residual moveout (Fig. 4). The back projection data are fed both into ray-based and a wavepath-based tomographic workflow. The inversion contains about 22,000 back projection points and the back projection paths cover an offset range of 15 km. The velocity model and hence the wavefields are sampled at 12.5 m vertically and 25 m horizontally. Both methods pick up lowered velocities below the base of salt, but only the wavepath inversion comes close to resolve the magnitude near the salt base and the fact that there is a low velocity zone extending to greater depth. The location of the subsalt low velocity zone, indicative of overpressure, is well resolved (upper image of Fig. 4).

Discussion

In areas of complex velocity that are challenging for raytracing based velocity inversion methods, wavepath tomography offers a naturally regularized alternative that is consistent with the wavefield continuation migration method used to produce the seismic image. The expense of computing a single wavepath kernel is partially offset, in comparison to ray tomography, by the smaller number of backprojections necessary to sample the velocity model adequately.

In practice, one will always reserve the expensive wavepath tomography for the parts of the velocity model that cannot be obtained by ray tomography and use ray tomography everywhere else. Submitting the wavepath and ray back projection equations together to the tomographic solver makes it easy to combine the two approaches. For example, in the Sigsbee case discussed before, the sedimentary velocities outside the salt body can easily be obtained from ray tomography. Even if the velocity field is very smooth and simple as is the case of Sigsbee, wavepath tomography adds robustness to the inversion because it does not have a problem with erratic ray paths resulting from multiple internal or “underside” reflections generated by the high velocity contrast between the sediments and the salt body or strong deflections of the ray path due to a rugose salt boundary.

Conclusion

We demonstrate that the method yields results superior to ray tracing in areas of complex overburden. In our example, the low velocity overpressure zone below a complex salt body is well resolved by wavepath tomography, illustrating the methods utility not only for velocity model building, but also for hazard detection.

Acknowledgements

We thank the SMAART JV and BP for the synthetic data sets used in this paper.

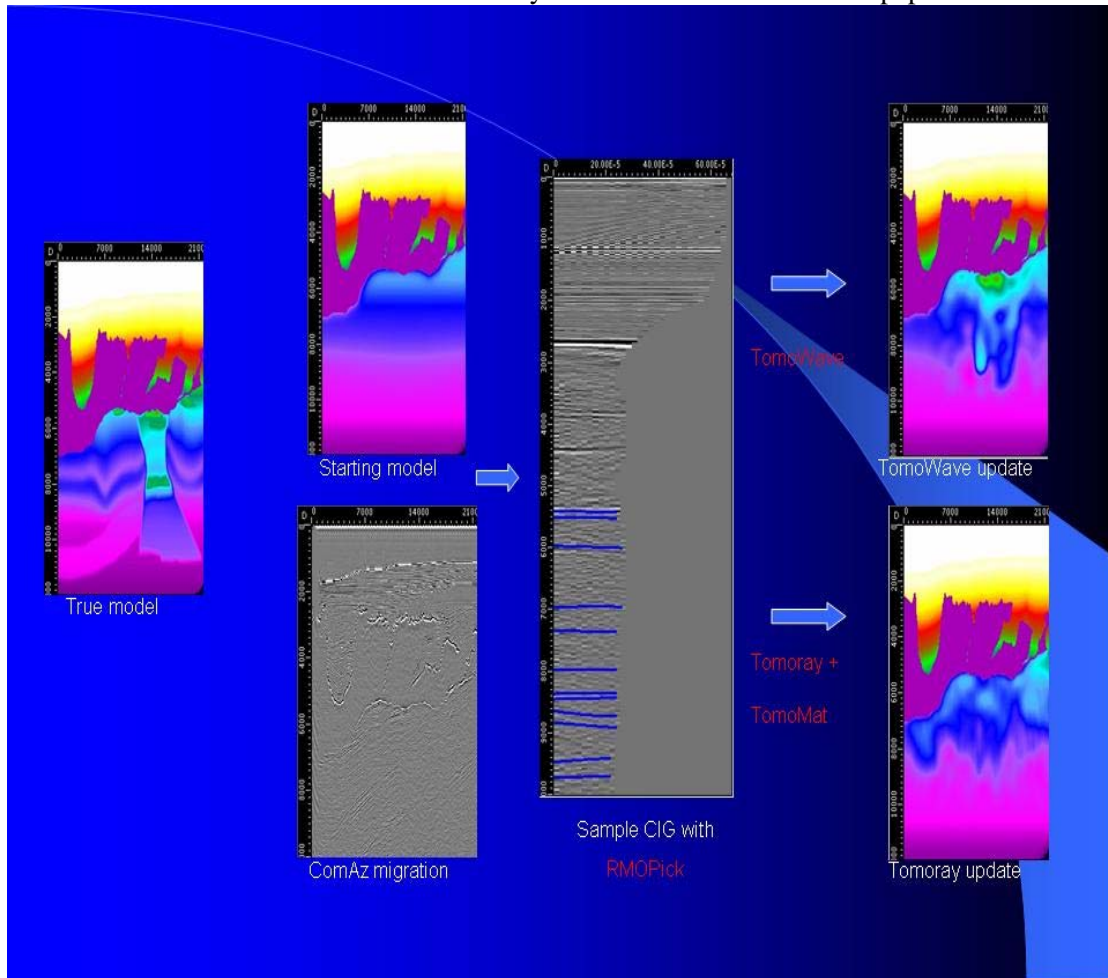


Figure 4. Results of ray tomography and wavepath tomography for detection of subsalt low velocity zones. Wavepath tomography based on actual subsalt residual moveout measured from the angle gathers is able to accurately detect and delineate the potential drilling hazard.

References

- Bevc, D., Fliedner, M. and VanderKwaak, J. [2006] 3-D tomographic updating with automatic volume-based picking. *76th Mtg. Soc. of Expl. Geophys.*, Expanded Abstracts, 3330-3334.
- Biondi, B. and Palacharla, G. [1996] 3D prestack migration of common-azimuth data. *Geophysics*, **61**, 1822—1832.
- Brown, M.P., Morton, S.A. and Whittle, G. [2006] Seismic event tracking by global path optimization. *76th Mtg. Soc. of Expl. Geophys.*, Expanded Abstracts, 1063-1067.
- Clapp, R.G., Biondo, B.L., Fomel, S.B. and Claerbout, J.F. [1998] Regularizing velocity estimation using geologic dip information. *68th Mtg. Soc. of Expl. Geophys.*, Expanded Abstracts, 1851-1854.
- Woodward, M.J. [1989] *Wave-Equation Tomography*. PhD Thesis, Stanford.